

Quantum Stopwatch: How To Store Time in a Quantum Memory

Yuxiang Yang,¹ Giulio Chiribella,^{1,2} and Masahito Hayashi^{3,4}

¹*Department of Computer Science, The University of Hong Kong, Pokfulam Road, Hong Kong*

²*Canadian Institute for Advanced Research, CIFAR Program in Quantum Information Science, Toronto, ON M5G 1Z8*

³*Graduate School of Mathematics, Nagoya University, Nagoya, Japan*

⁴*Centre for Quantum Technologies, National University of Singapore, Singapore*

Atomic clocks are Nature’s most accurate indicators of time. Still, their accuracy is subject to a fundamental quantum limit, known as the Heisenberg limit. When the readings of multiple clocks are combined together, as in the case of GPS networks, the intrinsic quantum errors accumulate, leading to a growing inaccuracy when the complexity of the setup increases. Here we introduce a method that eludes the accumulation of errors by coherently storing time in a quantum memory. The method is based on a quantum stopwatch mechanism, which achieves Heisenberg scaling with the size of the memory and is robust to noise. The quantum stopwatch can be used to measure the total duration of a sequence of events with the ultimate quantum accuracy, to engineer new states for quantum metrology, and to boost the performance of quantum sensor networks.

INTRODUCTION

Towards the end of the nineteenth century, Lord Kelvin suggested that atoms could be used as standard clocks, whose frequency will “*remain the same so long as the particles themselves exist*” [1]. Atomic clocks [2], building upon Lord Kelvin’s early idea, have become one of the most successful quantum technologies, offering spectacular accuracy [3–5] for a vast range of applications [6–9]. Still, there exists a limit that no technology can overcome. The limit has its roots in Heisenberg’s uncertainty principle, which entails an unavoidable error in the read-out of time [10–14]. The errors add up when the readings of multiple clocks are combined together, as in the case of GPS networks, and the situation becomes more severe as the complexity of the applications increases. To address this problem, one may try to eliminate all unnecessary measurements: instead of measuring individual clocks, one could store their state into the memory of a quantum computer, process all the data coherently, and finally read out the desired information with a single measurement. However, this approach is limited by the availability of quantum memories, which are notoriously expensive and hard to scale up [15]. Since atomic clocks typically consist of thousands of identical atoms [16], directly storing their state into a memory is beyond any technology that can be expected in the near future. As a result, it is vital to reduce the amount of memory used to store time information. This is not only an engineering problem—at the most fundamental level, the question is: how much memory is required to record time?

Here we derive the ultimate quantum limit on the amount of memory needed to record time with a prescribed accuracy. The limit is tight: we construct an explicit protocol where the memory size has the best possible scaling with the clock accuracy. Our protocol is the quantum analogue of a stopwatch, which records the duration of events into the state of a digital memory (see

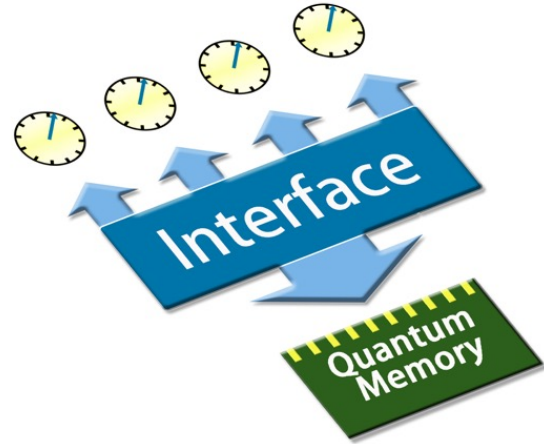


FIG. 1. **Working principle of the quantum stopwatch.** The quantum stopwatch coherently transfers time information from an atomic clock, consisting of many identical atoms, to a quantum memory, whose size has the ultimate quantum scaling with the accuracy of the clock.

Figure 1). The relation between accuracy and memory size can be regarded as a manifestation of Heisenberg’s fundamental limit. And yet, we find out a crucial difference between the Heisenberg scaling with the memory size and the familiar Heisenberg scaling of quantum metrology [17, 18]: while the latter requires entanglement in the clock, the latter can be attained even if the clock consists of many independently prepared atoms. As a result, the Heisenberg scaling with the memory is robust to depolarization and particle loss, two processes that are known to destroy the Heisenberg scaling with the clock size [19].

Storing time into a quantum memory of Heisenberg-limited size is a useful primitive for many applications. As an illustration, we construct a quantum-enhanced protocol to measure the total duration of a sequence of

events, such as a spike train generated by a neuron, or the activity of a search engine in response to a series of requests. Other applications include the generation of new quantum states with Heisenberg-limited sensitivity and the realization of large-scale quantum sensor networks.

RESULTS

Heisenberg limit on the memory size. Suppose that information about a real parameter T is stored in the state of a quantum memory. When needed, the memory is accessed by a quantum measurement, producing an estimate \hat{T} . The accuracy of the measurement can be quantified by the size of the smallest interval, centred around the true value, in which the estimate falls with a prescribed probability P —for example, $P = 99\%$. Explicitly, the size of the interval is

$$\delta(P, T) := \min \left\{ \delta \mid \text{Prob} \left(\left| \hat{T} - T \right| \leq \frac{\delta}{2} \right) \geq P \right\}. \quad (1)$$

The dependence on the true value can be removed by fixing a fiducial interval $[T_{\min}, T_{\max}]$ and evaluating the worst-case of $\delta(P, T)$ within that interval. We denote the worst-case accuracy as $\delta(P)$.

Now, there exists a fundamental relation between accuracy and memory size, quantified by the number M of distinct orthogonal states used in the encoding. The relation is

$$\delta(P) \geq \frac{P \Delta T}{M + 1}, \quad (2)$$

with $\Delta T = T_{\max} - T_{\min}$. Eq. (2) shows that the inaccuracy $\delta(P)$ cannot vanish faster than $1/M$ with the memory size.

The bound (2) follows from dividing the fiducial interval into $N = \lfloor \Delta T / \delta(P) \rfloor$ disjoint intervals of size $\delta(P)$. For the i -th interval, one can encode the midpoint value T_i into the state of the memory. In this way, one obtains N quantum states that, by construction, can be distinguished with probability of success at least P . On the other hand, the N states are contained in an M -dimensional space, and therefore the probability of success is upper bounded by M/N [20], leading to the bound $P \leq M/N$ and, in turn, to Eq. (2).

The Heisenberg scaling with the memory size implies that the minimum number of memory qubits Q needed to achieve accuracy $\delta(P)$ is lower bounded as

$$Q \geq \log \frac{1}{\delta(P)} \quad (3)$$

at the leading order. We call Eq. (3) the *Heisenberg limit on the memory size*. In the following, we show that the Heisenberg limit is tight and can be attained also in the presence of noise.

Noisy clock model. Consider an atomic clock made of n identical atoms (or ions) oscillating between two

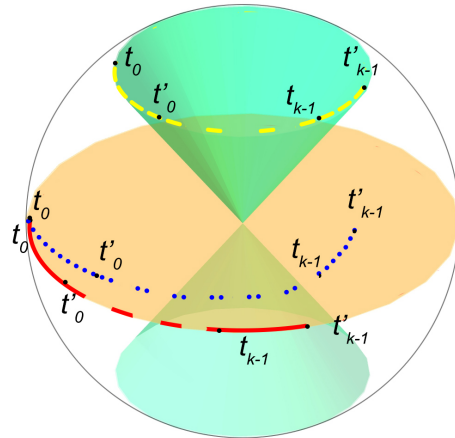


FIG. 2. Evolution of a clock qubit. The figure illustrates the evolution of a clock qubit in three different scenarios. The red, solid curve on the equator of Bloch sphere represents the trajectory of a clock qubit with $s = 1/2$, evolving under noiseless evolution ($\gamma = 0$). The blue, dotted curve represents the trajectory of a clock qubit, initially on the equator ($s = 1/2$), spiralling toward the centre of the Bloch sphere due to depolarizing noise with $\gamma > 0$. The yellow, dashed curve corresponds to a clock qubit with latitude parameter $s > 1/2$ and noiseless evolution ($\gamma = 0$).

energy levels. Restricting the attention to these levels, each atom can be modelled as a qubit. In the absence of noise, the evolution of each qubit is governed by the Hamiltonian $H = E_0 |0\rangle\langle 0| + E_1 |1\rangle\langle 1|$, where E_0 and E_1 are the energy levels, corresponding to the eigenstates $|0\rangle$ and $|1\rangle$, respectively. In practice, however, noise is inevitable. The typical example of noisy process is depolarization, which perturbs the state of the clock, eventually degrading it to the maximally mixed state. Taking depolarization into account, the evolution is described by the master equation [12]

$$\frac{d\rho_t}{dt} = \frac{i}{\hbar} [H, \rho_t] + \frac{\gamma}{4} \sum_{i=x,y,z} (\sigma_i \rho_t \sigma_i - \rho_t), \quad (4)$$

where σ_x, σ_y , and σ_z are the three Pauli matrices and $\gamma \geq 0$ is the decay rate, corresponding to the inverse of the relaxation time T_2 in NMR. The master equation leads to an effective time evolution [21, 22], whereby a clock, initially in the pure state $|\varphi_0\rangle = \sqrt{s}|0\rangle + \sqrt{1-s}|1\rangle$, evolves to the mixed state

$$\rho_{t,\gamma} := e^{-\gamma t} |\varphi_t\rangle\langle\varphi_t| + (1 - e^{-\gamma t}) \frac{I}{2}, \quad (5)$$

with $|\varphi_t\rangle := \sqrt{s}|0\rangle + \sqrt{1-s}e^{-it}|1\rangle$ (here we set $(E_1 - E_0)/\hbar = 1$ for simplicity). A pictorial representation of the evolution is provided in Figure 2.

Efficient storage of time information. Our goal is to store time into a quantum memory of Heisenberg-limited

size. To this purpose, we devise a quantum compression protocol that stores the state of n clock qubits into $1/2 \log n$ memory qubits at the leading order. In this way, the time information contained into thousands of clock qubits can be faithfully stored into a few tens of memory qubits. The advantage can already be observed for small clocks: for example, a quantum clock consisting of four pure qubits on the equator of the Bloch sphere can be encoded into only two memory qubits with fidelity 87.9%.

The storage of time information is implemented in three steps. The first step is to perform the Schur transform [23], a reversible process that converts the state of the n clock qubits into a state of three quantum registers: the index register, the representation register, and the multiplicity register. The index register contains information about the total spin J , ranging from $J = 0$ to $J = n/2$ when n is even. The representation register contains the time information, while the multiplicity register is irrelevant and is discarded. The second step is to read out the value of the total spin from the index register and to store the result in a classical memory of $\log(n/2 + 1)$ bits. As a result of the measurement, the representation register ends up in the state $\rho_{t,\gamma,J}$, where J is the outcome read from the index register. The two steps presented so far are not specific to clock states: they could also be used to compress arbitrary qubit states [24, 25]. The third step, instead, is tailor-made for clock states. It compresses the representation register into a quadratically smaller system, by getting rid of the highest and lowest frequency modes in the state $\rho_{t,\gamma,J}$. We call this technique *frequency projection*.

The key idea of frequency projection is that the density matrix $\rho_{t,\gamma,J}$ has support in a $(2J + 1)$ -dimensional subspace spanned by the basis states $\{|J, m\rangle\}_{m=-J}^J$, with the state $|J, m\rangle$ corresponding to the m -th frequency mode of the noiseless evolution. Frequency projection consists in getting rid of all the frequencies outside an interval of size $\sqrt{J} \log J$ centred around the value $m_0 = (2s - 1)J$. Since J is at most equal to $n/2$, this means that the state is projected into a subspace of size $\sqrt{n} \log n + O(1)$. Hence, the number of memory qubits needed to store the projected state is $1/2 \log n$ at the leading order.

The central result about frequency projection is that it is asymptotically faithful: for large J , the projected state is almost indistinguishable from the original state. In Appendix A, we show that the trace distance between the two states is upper bounded as

$$\epsilon_{J,t,\gamma}^{\text{proj}} \leq \frac{3}{2} J^{-\frac{1}{8} \ln \coth \frac{\gamma t}{2}} + O\left(J^{-\frac{1}{8} \ln J}\right). \quad (6)$$

Note that error vanishes in the large J limit, provided that the time t is not too large compared to the relaxation time $T_2 = 1/\gamma$. This condition simply means that the clock qubits work for the time scale relevant in the experiment. Averaging over J , we obtain that the overall

error vanishes in the large n limit (see Appendix B).

Attainability of the Heisenberg limit. We now show that our compression protocol achieves Heisenberg scaling with the size of the memory. In order to read out time, we first transfer the time information from the memory back to the clock qubits. Then, we measure the clock qubits with a simple measurement strategy, which does not require entanglement or adaptive operations: in order to estimate time, each clock qubit is measured independently. Specifically, the i -th qubit is measured on the eigenstates of the observable $O_i = \cos \tau_i \sigma_X + \sin \tau_i \sigma_Y$, where τ_i is a random angle, chosen independently for every qubit. The measurement has two possible outcomes, $+1$ and -1 . If the outcome of the measurement is $+1$, one records the value τ_i , if the outcome is -1 , one records the value $\tau_i + \pi$. By collecting the results from all qubits, one obtains a vector $\vec{\tau}$ of n independent and identically distributed random outcomes. At this point, an estimate of time can be obtained through the maximum likelihood technique.

To evaluate the error in the readout, it is convenient to first neglect the compression errors. In this setting, the probability that the maximum likelihood estimate \hat{T} deviates from the true value by less than δ is [26]

$$\text{Prob}\left(|\hat{T} - T| \leq \frac{\delta}{2}\right) = \text{erf}\left(\delta \sqrt{\frac{n F_{\text{loc}}}{8}}\right) + \epsilon_n, \quad (7)$$

where $\text{erf}(x)$ is the error function of the normal distribution, F_{loc} is the classical Fisher information (see Methods for the explicit expression), and ϵ_n is a small correction of size $1/\sqrt{n}$. For any probability threshold P , the accuracy can be expressed as

$$\delta(P) = \sqrt{\frac{8}{n F_{\text{loc}}}} \text{erfc}^{-1}(P) \quad (8)$$

at the leading order. Now, compression introduces an error that vanishes in the large n limit. Hence, a time measurement performed on the recovered state has approximately the same statistics of a time measurement in the absence of compression errors. Quantitatively, the probability that the measurement outcome falls within an interval of size δ around the true value is lower bounded by the same term in the r.h.s. of Eq. (7), plus a small correction that vanishes in the large n limit. As a result, the accuracy still has the scaling $\delta(P) = c/\sqrt{n}$ for some suitable constant c . In terms of memory size, this shows that our compression protocol achieves the Heisenberg limit (3). Indeed, the protocol uses $Q = 1/2 \log n$ memory qubits at the leading order and the scaling with the accuracy is exactly the Heisenberg scaling $Q = \log[1/\delta(P)]$.

Application: measuring the duration of a sequence of events. Our quantum stopwatch protocol can be used as a primitive in several applications. As

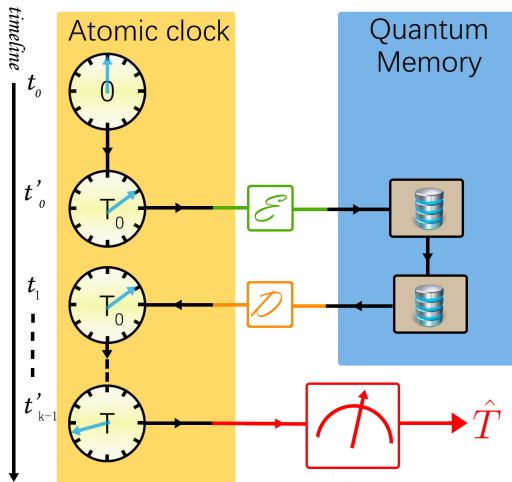


FIG. 3. **Coherent protocol measuring the total duration of k events.** The clock starts its time evolution at time t_0 and continues evolving until time t'_0 , when the first event is concluded. At this point, the time information is encoded in the quantum memory for storage until time t_1 , when the state is released from the memory and the evolution of the clock resumes. The procedure is repeated for k times, so that the total duration of the k events is coherently recorded in the state of the memory. Finally, the state of the memory is measured, yielding an estimate of the total duration.

an illustration, we construct a quantum setup that coherently measures the total duration of a sequence of k events. The setup uses a quantum clock made of n identical qubits. At time t_0 , each qubit is initialized in the state $\rho_{t_0, \gamma}$. The qubit evolves until time $t'_0 = t_0 + T_0$ under the noisy dynamics (4). The state of the n clock qubits is then stored in the quantum memory, where it remains until t_1 , when it is released and resumes its evolution until t'_1 . The procedure is iterated for k times, so that in the end the state of the clock records the total duration of the k events. At this point, the clock is measured and an estimate of the total duration is produced. An illustration of the steps in the protocol is provided in Figure 3.

Our coherent setup offers an advantage over incoherent protocols, where k measurements are performed, the outcomes are stored in a classical memory, and the sum is computed by classical means. In the noiseless case ($\gamma = 0$), the comparison between is straightforward: performing a single measurement instead of k measurements increases the accuracy by a factor \sqrt{k} . This advantage arises also in the task of measuring the duration of a process by probing it for k times. Classically, k repetitions of the same experiment lead to an increase of the accuracy by a factor \sqrt{k} . In contrast, the coherent protocol increases the accuracy by a factor of k .

The benefits of the coherent protocol are not limited

to the noiseless scenario. A performance comparison between coherent and incoherent protocols is presented in Figure 4, showing the advantage of the coherent approach. In addition, we analytically prove that the co-

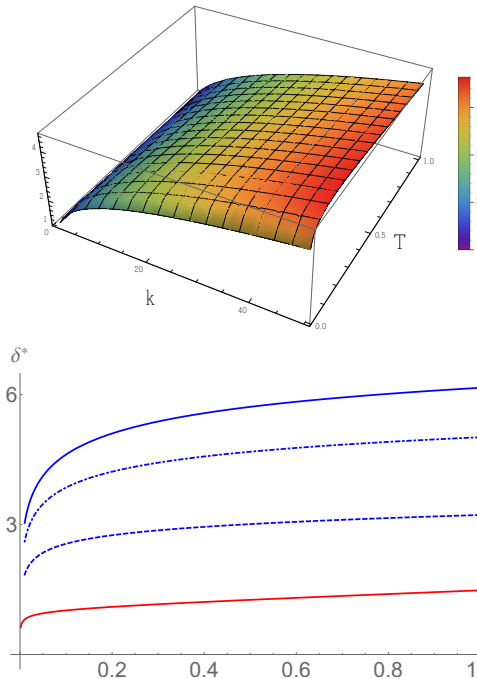


FIG. 4. **Comparison between coherent and incoherent protocols.** *On the top:* ratio between the inaccuracy of the incoherent protocol and the inaccuracy of the coherent protocol. The figure shows the ratio for equatorial qubits with decay rate $\gamma = 0.2$. The quantum advantage grows with the number of time intervals k , with an inaccuracy reduction of about 5 times for $k = 50$. *On the bottom:* Dependence of the rescaled inaccuracy $\delta^* = \sqrt{n} \delta$ on the total time T . For the coherent protocol (red line) the inaccuracy is independent of k , while incoherent protocols have inaccuracies increasing with k , illustrated by the blue lines for $k = 10, 30$, and 50 .

herent protocol has better performance than protocols using only classical memories whenever the condition

$$k \geq \frac{1 + \gamma^2 / \sqrt{1 - 4s(1-s)}}{1 - \sqrt{1 - 4s(1-s)} e^{-2\gamma T}} \quad (9)$$

is satisfied (see Appendix C). In other words, the total duration of a sequence of events is better computed coherently whenever the number of events is large.

DISCUSSION

The coherent storage of time in a quantum memory promises a number of advantages for quantum metrology. It is then important to assess its experimental feasibility. The initialization of the clock and the final measurement are standard routines in Ramsey spectroscopy

and they can be implemented with great accuracy [2]. The compression protocol can be broken down into two main ingredients: the Schur transform and the frequency projection. The Schur transform can be efficiently realized by a quantum circuit of at most polynomially many gates [23]. The circuit is simpler in the noiseless case [27] and has been recently implemented in a prototype photonic setup [28]. The frequency projection can be efficiently implemented with a technique introduced in Ref. [27], whereby the basis state $|J, m\rangle$ is encoded into a $(2J + 1)$ -qubit state, with the m -th qubit is in the state $|1\rangle$ and all the other qubits are in the state $|0\rangle$. In this encoding, projecting on a restricted range of values of m is the same as throwing away some of the qubits. The encoding operations and their inverses can be implemented using $O(j^2)$ elementary gates [27]. In summary, all the components of the quantum stopwatch can be implemented efficiently, suggesting that our protocol may be experimentally demonstrated in the near future. The benefits of the quantum stopwatch give further motivation to the realization of long-lived quantum memories and high-fidelity storage/retrieval operations, two very active research directions in experimental quantum information science [29–34].

The techniques introduced in this paper benefit a broad range of applications. For example, frequency projection offers the opportunity to transform product states of n qubits into entangled states of \sqrt{n} qubits, allowing one to reversibly switch from an encoding where the information can be accessed locally to a more compact encoding where the information is available globally. This primitive can be employed to generate new states with Heisenberg-limited sensitivity, by first preparing product states and then eliminating the extreme frequencies.

Another application is the ultraprecise measurement of time in quantum sensor networks. Consider for example the network of quantum clocks proposed in Refs. [35, 36]. The network consists of k spatially separated nodes, which cooperate to establish a global time standard. To this purpose, the nodes utilize n copies of the GHZ state $|\text{GHZ}\rangle = (|0\rangle^{\otimes k} + |1\rangle^{\otimes k})/\sqrt{2}$, which they receive from a central station. Using our frequency projection technique, it is possible to compress the n copies into a multipartite entangled state of exponentially smaller size, so that each node has a local clock of $1/2 \log n$ qubits. Exploiting this fact, one can obtain the same precision of Refs. [35, 36] using an exponentially smaller amount of quantum communication between the nodes and the central station, as illustrated in Figure 5.

Finally, the ability to store clock states into the minimum amount of memory could pave the way to the design of autonomous quantum machines equipped with an internal clock, or learning machines that can record to the duration of events happening in their surroundings.

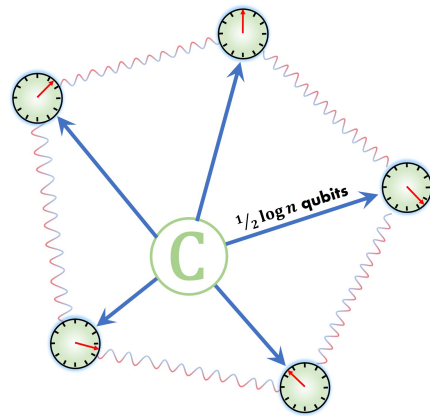


FIG. 5. **Boosting the performance of quantum sensor networks.** A central station C distributes quantum information to k nodes, generating entanglement among k local clocks. Using frequency projection, the central station distributes a quantum state that guarantees the same precision of n GHZ states, while requiring an exponentially smaller amount of quantum communication of $1/2 \log n$ qubits per node.

METHODS

Precision analysis. Here we assess the accuracy of the time measurement used in the quantum stopwatch protocol. We first analyze the scenario where the decay rate γ is known and then extend the analysis to unknown decay rate.

Precision assessment with known decay rate. In the stopwatch protocol, the estimate of time is produced by performing n independent random measurements on n identically prepared qubits. Mathematically, each random measurement is described by the positive operator-valued measure $\{M_\tau\}_{\tau \in [0, 2\pi]}$ with

$$M_\tau = \frac{1}{2\pi} \begin{pmatrix} 1 & e^{-i\tau} \\ e^{i\tau} & 1 \end{pmatrix}. \quad (10)$$

The probability density that the measurement yields outcome τ when the input state is $\rho_{T,\gamma}$ is $P_{T,\gamma}(\tau) := \text{Tr}[\rho_{T,\gamma} M_\tau]$. The inaccuracy of this measurement, denoted by $\delta_{\text{loc}}(P)$, can be expressed as

$$\delta_{\text{loc}}(P) = \sqrt{\frac{8}{nF_{\text{loc}}}} \text{erf}^{-1}(P) + o\left(\frac{1}{\sqrt{n}}\right) \quad (11)$$

where F_{loc} is the classical Fisher information of the probability distribution $P_{T,\gamma}(\tau)$, given by

$$F_{\text{loc}} = 1 - \gamma^2 - \sqrt{1 - 4s(1-s)e^{-2\gamma T}} + \frac{\gamma^2}{\sqrt{1 - 4s(1-s)e^{-2\gamma T}}}. \quad (12)$$

Let us analyze the performance of the optimal strategy using arbitrary quantum measurements. The inaccuracy

of the optimal strategy $\delta_{\text{opt}}(P)$ is still given by the expression (11), with F_{loc} replaced by the quantum Fisher information F_{Q} , given by

$$F_{\text{Q}} = 4s(1-s)e^{-2\gamma T} + \frac{\gamma^2}{e^{2\gamma T} - 1} \quad (13)$$

where s is the parameter specifying the initial state (see Appendix D).

Comparing Eqs. (12) and (13), one can see that the advantage of adaptive measurements is limited. Indeed, the ratio between the inaccuracies of the local strategy and of the optimal quantum strategy is upper bounded as

$$\frac{\delta_{\text{loc}}(P)}{\delta_{\text{opt}}(P)} \leq \sqrt{2} \cdot \sqrt{\frac{1 + \gamma^2/[4s(1-s)(1 - e^{-2\gamma T})]}{1 + \gamma^2}} \quad (14)$$

at the leading order in n (see Appendix E). In the absence of noise ($\gamma = 0$), the above bound shows that the local strategy based on random single-qubit measurements has an inaccuracy at most $\sqrt{2}$ times that of the optimal measurement. In general, Eq. (14) shows the inaccuracy of the local strategy is within a constant times that of the optimal strategy, for all values of T larger than a minimum time $T_{\text{min}} > 0$.

Precision assessment with unknown decay rate. The optimal strategy for estimating the duration T depends on the decay rate γ . When γ is unknown, it must be treated as a *nuisance parameter* [37], namely a parameter that is not directly of interest but affects the analysis of the data. In this case, the inaccuracy of the local strategy is determined by Eq. (11) with the Fisher information replaced by the quantity $1/(F_{\text{loc}}^{-1})_{TT}$, i.e. $\delta_{\text{loc}}(P) \propto \sqrt{(F_{\text{loc}}^{-1})_{TT}/n}$, where F_{loc} is now the Fisher information matrix [38]. In Appendix F, we derive the explicit form of this entry as

$$(F_{\text{loc}}^{-1})_{TT} = \frac{1}{1 - \sqrt{1 - 4s(1-s)e^{-2\gamma T}}}. \quad (15)$$

We now compare Eq. (15) with the precision of the optimal quantum strategy. For the latter case, the inaccuracy $\delta_{\text{opt}}(P)$ is proportional to the square root of the quantity $(F_{\text{Q}}^{-1})_{TT}$, where F_{Q} is now the quantum Fisher information matrix [39, 40]. In Appendix G, we show that

$$(F_{\text{Q}}^{-1})_{TT} = \frac{1}{4s(1-s)e^{-2\gamma T}}. \quad (16)$$

Comparing Eqs. (15) and (16), we obtain that the ratio between the inaccuracies is upper bounded as

$$\frac{\delta_{\text{loc}}(P)}{\delta_{\text{opt}}(P)} \leq \sqrt{2} \quad (17)$$

at the leading order, for all possible values of the time T and of the decay rate γ . Again, the advantage of the optimal measurement is limited by a constant factor.

-
- [1] Kelvin, W. T. B. & Tait, P. G. *Elements of natural philosophy*, vol. 23 (Amer. home lib., 1902).
 - [2] Ludlow, A. D., Boyd, M. M., Ye, J., Peik, E. & Schmidt, P. O. Optical atomic clocks. *Reviews of Modern Physics* **87**, 637 (2015).
 - [3] Chou, C., Hume, D., Koelemeij, J., Wineland, D. & Rosenband, T. Frequency comparison of two high-accuracy Al⁺ optical clocks. *Physical Review Letters* **104**, 070802 (2010).
 - [4] Ushijima, I., Takamoto, M., Das, M., Ohkubo, T. & Katori, H. Cryogenic optical lattice clocks. *Nature Photonics* **9**, 185–189 (2015).
 - [5] Huntemann, N., Sanner, C., Lipphardt, B., Tamm, C. & Peik, E. Single-ion atomic clock with 3×10^{-18} systematic uncertainty. *Physical review letters* **116**, 063001 (2016).
 - [6] Giovannetti, V., Lloyd, S. & Maccone, L. Quantum-enhanced positioning and clock synchronization. *Nature* **412**, 417–419 (2001).
 - [7] Santarelli, G. *et al.* Quantum projection noise in an atomic fountain: A high stability cesium frequency standard. *Physical Review Letters* **82**, 4619 (1999).
 - [8] Steinmetz, T. *et al.* Laser frequency combs for astronomical observations. *Science* **321**, 1335–1337 (2008).
 - [9] Li, C.-H. *et al.* A laser frequency comb that enables radial velocity measurements with a precision of 1 cm s^{-1} . *Nature* **452**, 610–612 (2008).
 - [10] Chuang, I. L. Quantum algorithm for distributed clock synchronization. *Physical Review Letters* **85**, 2006 (2000).
 - [11] Jozsa, R., Abrams, D. S., Dowling, J. P. & Williams, C. P. Quantum clock synchronization based on shared prior entanglement. *Physical Review Letters* **85**, 2010 (2000).
 - [12] Huelga, S. F. *et al.* Improvement of frequency standards with quantum entanglement. *Physical Review Letters* **79**, 3865 (1997).
 - [13] Smirne, A., Kołodyński, J., Huelga, S. F. & Demkowicz-Dobrzański, R. Ultimate precision limits for noisy frequency estimation. *Physical Review Letters* **116**, 120801 (2016).
 - [14] Bužek, V., Derka, R. & Massar, S. Optimal quantum clocks. *Physical Review Letters* **82**, 2207 (1999).
 - [15] Simon, C. *et al.* Quantum memories. *The European Physical Journal D* **58**, 1–22 (2010).
 - [16] Nicholson, T. *et al.* Systematic evaluation of an atomic clock at 2×10^{-18} total uncertainty. *Nature Communications* **6** (2015).
 - [17] Giovannetti, V., Lloyd, S. & Maccone, L. Quantum metrology. *Physical Review Letters* **96**, 010401 (2006).
 - [18] Giovannetti, V., Lloyd, S. & Maccone, L. Advances in quantum metrology. *Nature Photonics* **5**, 222–229 (2011).
 - [19] Demkowicz-Dobrzański, R., Kołodyński, J. & Guţă, M. The elusive heisenberg limit in quantum-enhanced metrology. *Nature Communications* **3**, 1063 (2012).
 - [20] Yuen, H., Kennedy, R. & Lax, M. Optimum testing of

- multiple hypotheses in quantum detection theory. *IEEE Transactions on Information Theory* **21**, 125–134 (1975).
- [21] Romero, K. F. & Franco, R. L. Simple non-markovian microscopic models for the depolarizing channel of a single qubit. *Physica Scripta* **86**, 065004 (2012).
- [22] Arsenijević, M., Jeknić-Dugić, J. & Dugić, M. Generalized kraus operators for the one-qubit depolarizing quantum channel. *Brazilian Journal of Physics* **47**, 339–349 (2017). URL <http://dx.doi.org/10.1007/s13538-017-0502-3>.
- [23] Bacon, D., Chuang, I. L. & Harrow, A. W. Efficient quantum circuits for Schur and Clebsch-Gordan transforms. *Physical Review Letters* **97**, 170502 (2006).
- [24] Blume-Kohout, R., Croke, S. & Zwolak, M. Quantum data gathering. *Scientific reports* **3** (2013).
- [25] Yang, Y., Chiribella, G. & Ebler, D. Efficient quantum compression for ensembles of identically prepared mixed states. *Physical Review Letters* **116**, 080501 (2016). URL <http://link.aps.org/doi/10.1103/PhysRevLett.116.080501>.
- [26] Van der Vaart, A. W. *Asymptotic statistics*, vol. 3 (Cambridge university press, 2000).
- [27] Plesch, M. & Bužek, V. Efficient compression of quantum information. *Physical Review A* **81**, 032317 (2010).
- [28] Rozema, L. A., Mahler, D. H., Hayat, A., Turner, P. S. & Steinberg, A. M. Quantum data compression of a qubit ensemble. *Physical Review Letters* **113**, 160504 (2014). URL <http://link.aps.org/doi/10.1103/PhysRevLett.113.160504>.
- [29] Bao, X.-H. *et al.* Efficient and long-lived quantum memory with cold atoms inside a ring cavity. *Nature Physics* **8**, 517–521 (2012).
- [30] Mouradian, S. L. *et al.* Scalable integration of long-lived quantum memories into a photonic circuit. *Physical Review X* **5**, 031009 (2015).
- [31] Natterer, F. D. *et al.* Reading and writing single-atom magnets. *Nature* **543**, 226228 (2017).
- [32] England, D. G. *et al.* Storage and retrieval of THz-bandwidth single photons using a room-temperature diamond quantum memory. *Physical Review Letters* **114**, 053602 (2015).
- [33] Fisher, K. A. *et al.* Frequency and bandwidth conversion of single photons in a room-temperature diamond quantum memory. *Nature Communications* **7** (2016).
- [34] Distanto, E. *et al.* Storing single photons emitted by a quantum memory on a highly excited Rydberg state. *Nature Communications* **8** (2017).
- [35] Komar, P. *et al.* A quantum network of clocks. *Nature Physics* **10**, 582–587 (2014).
- [36] Kómár, P. *et al.* Quantum network of atom clocks: A possible implementation with neutral atoms. *Physical Review Letters* **117**, 060506 (2016). URL <http://link.aps.org/doi/10.1103/PhysRevLett.117.060506>.
- [37] Young, G. A. & Smith, R. L. *Essentials of statistical inference*, vol. 16 (Cambridge University Press, 2005).
- [38] Cramér, H. *Mathematical Methods of Statistics*, vol. 9 (Princeton university press, 2016).
- [39] Helstrom, C. W. *Quantum detection and estimation theory* (Academic press, 1976).
- [40] Gill, R. D. & Massar, S. State estimation for large ensembles. *Physical Review A* **61**, 042312 (2000).
- [41] Fulton, W. & Harris, J. *Representation theory*, vol. 129 (Springer Science & Business Media, 1991).
- [42] Hayashi, M. *Group Representation for Quantum Theory* (Springer, 2017).
- [43] Winter, A. Coding theorem and strong converse for quantum channels. *IEEE Transactions on information theory* **45**, 2481 (1999).
- [44] Wilde, M. *Quantum information theory* (Cambridge University Press, 2013).
- [45] Yang, Y., Chiribella, G. & Hayashi, M. Optimal compression for identically prepared qubit states. *Physical Review Letters* **117**, 090502 (2016). URL <http://link.aps.org/doi/10.1103/PhysRevLett.117.090502>.

Acknowledgments. This work is supported by the Hong Kong Research Grant Council through Grant No. 17326616, by National Science Foundation of China through Grant No. 11675136, by the HKU Seed Funding for Basic Research, the John Templeton Foundation, and by the Canadian Institute for Advanced Research (CIFAR). Y. Y. is supported by a Hong Kong and China Gas Scholarship. MH was supported in part by a MEXT Grant-in-Aid for Scientific Research (B) No. 16KT0017, a MEXT Grant-in-Aid for Scientific Research (A) No. 23246071, the Okawa Research Grant, and Kayamori Foundation of Informational Science Advancement. Centre for Quantum Technologies is a Research Centre of Excellence funded by the Ministry of Education and the National Research Foundation of Singapore. We thank Lorenzo Maccone for useful comments and Xinhui Yang for drawing the figures.

Author contributions. All authors contributed to the work presented in this paper.

Competing financial interests. The authors declare no competing financial interests.

Appendix A: error bound for frequency projection [Eq. (6) of the main text].

Here we prove Eq. (6) of the main text, regarding the error of frequency projection of the compressor. We prove the result in a general setting, where the states to be compressed are of the form

$$\rho_{\phi,p} := p|\phi\rangle\langle\phi| + (1-p)|\phi_{\perp}\rangle\langle\phi_{\perp}|, \quad (18)$$

with $p \in (1/2, 1]$, $|\phi\rangle = \sqrt{s}|0\rangle + \sqrt{1-s}e^{-i\phi}|1\rangle$, and $|\phi_{\perp}\rangle := \sqrt{1-s}|0\rangle - \sqrt{se^{-i\phi}}|1\rangle$ for some fixed $s \in (0, 1)$. Note that the clock states $\rho_{t,\gamma}$ considered in the main text are a special case of states of the form (18), with $p = (1 + e^{-\gamma t})/2$

and $\phi = t$.

To begin with, we recall a few basic facts from the main text. First, the n -fold clock state $\rho_{\phi,p}^{\otimes n}$ can be decomposed as

$$\rho_{\phi,p}^{\otimes n} \simeq \sum_{J=0}^{n/2} q_J \left(|J\rangle\langle J| \otimes \rho_{\phi,p,J} \otimes \frac{I_{m_J}}{m_J} \right), \quad (19)$$

where \simeq denotes the unitary equivalence implemented by the Schur transform, J is the quantum number of the total spin, $q_{J,t,\gamma}$ is a probability distribution, $|J\rangle$ is the state of the index register, $\rho_{t,\gamma,J}$ is the state of the representation register, and I_{m_J}/m_J is the maximally mixed state in a suitable subspace of the multiplicity register [41, 42]. The state $\rho_{\phi,p,J}$ can be expressed in the form

$$\rho_{\phi,p,J} = U_{\phi}^{\otimes n} (\rho_{p,J}) U_{\phi}^{\dagger \otimes n} \quad U_{\phi} = |0\rangle\langle 0| + e^{i\phi}|1\rangle\langle 1|, \quad (20)$$

where the fixed state $\rho_{p,J}$ has the form

$$\rho_{p,J} := (N_J)^{-1} \sum_{m=-J}^J p^{J+m}(1-p)^{J-m} |J, m\rangle_s \langle J, m|_s \quad (21)$$

$$N_J := \sum_{k=-J}^J p^{J+k}(1-p)^{J-k} \quad (22)$$

where $|J, m\rangle_s$ is the orthonormal basis defined as

$$|J, m\rangle_s := \frac{\sum_{\pi \in \mathcal{S}_{2J}} V_{\pi} |\phi_0\rangle^{\otimes (J+m)} |\phi_{0,\perp}\rangle^{\otimes (J-m)}}{\sqrt{(2J)!(J+m)!(J-m)!}} \quad (23)$$

with $|\phi_0\rangle = \sqrt{s}|0\rangle + \sqrt{1-s}|1\rangle$, $|\phi_{0,\perp}\rangle = \sqrt{1-s}|0\rangle - \sqrt{s}|1\rangle$, \mathcal{S}_{2J} being the $(2J)$ -symmetric group and V_{π} being the unitary implementing the permutation π .

The frequency projection channel $\mathcal{P}_{\text{proj},J}$ is defined as

$$\begin{aligned} \mathcal{P}_{\text{proj},J}(\rho) &:= P_{\text{proj},J} \rho P_{\text{proj},J} + (1 - \text{Tr}[\rho P_{\text{proj},J}]) \rho_0 \\ P_{\text{proj},J} &:= \sum_{|m-(2s-1)J| \leq \frac{\sqrt{J \log J}}{2}} |J, m\rangle\langle J, m|, \end{aligned} \quad (24)$$

where ρ_0 is a fixed state of the representation register. Eq. (7) of the main text is stated exactly by the following theorem.

Theorem 1. *For large J , the frequency projection error $\epsilon_{\text{proj},J} := \frac{1}{2} \|\mathcal{P}_{\text{proj},J}(\rho_{\phi,p,J}) - \rho_{\phi,p,J}\|_1$ is upper bounded as*

$$\epsilon_{\text{proj},J} \leq (3/2)J^{-\frac{1}{8}} \ln\left(\frac{p}{1-p}\right) + O\left(J^{-\frac{1}{8}} \ln J\right) \quad (25)$$

for every t .

The property below is useful in our proof of the error bound.

Lemma 1. *The basis $\{|J, m\rangle_s\}$ defined by Eq. (23) satisfies the property*

$$|\langle J, m|_s |J, k\rangle| \leq \begin{cases} \sqrt{\binom{2J}{J+k} \binom{2J}{J-m} s^{2J+k-m} (1-s)^{m-k}}, & s \geq 1/2 \\ \sqrt{\binom{2J}{J+k} \binom{2J}{J-m} s^{m+k} (1-s)^{2J-m-k}}, & s < 1/2. \end{cases} \quad (26)$$

where

$$|J, k\rangle := \frac{\sum_{\pi \in \mathcal{S}_{2J}} V_{\pi} |0\rangle^{\otimes (J+k)} |1\rangle^{\otimes (J-k)}}{\sqrt{(2J)!(J+k)!(J-k)!}}$$

is the symmetric basis.

Proof. Exploiting the symmetry of both bases, we have the following chain of inequalities.

$$|\langle J, m|_s|J, k\rangle| = \frac{1}{(2J)!} \left| \sum_{\pi, \pi' \in \mathcal{S}_{2J}} \frac{\langle \phi_0 |^{\otimes (J+m)} \langle \phi_{0,\perp} |^{\otimes (J-m)} V_\pi V_{\pi'} |0\rangle^{\otimes (J+k)} |1\rangle^{\otimes (J-k)} \rangle}{\sqrt{(J+m)!(J-m)!(J+k)!(J-k)!}} \right| \quad (27)$$

$$= \left| \sum_{\pi \in \mathcal{S}_{2J}} \frac{\langle \phi_0 |^{\otimes (J+m)} \langle \phi_{0,\perp} |^{\otimes (J-m)} V_\pi |0\rangle^{\otimes (J+k)} |1\rangle^{\otimes (J-k)} \rangle}{\sqrt{(J+m)!(J-m)!(J+k)!(J-k)!}} \right| \quad (28)$$

$$= \sqrt{\frac{(J+m)!(J-m)!}{(J+k)!(J-k)!}} \left| \sum_{l=\max\{0, -k-m\}}^{\min\{J-m, J-k\}} (-1)^l \binom{J-k}{l} \binom{J+k}{J-m-l} s^{\frac{2l+k+m}{2}} (1-s)^{\frac{2J-m-k-2l}{2}} \right| \quad (29)$$

$$\leq \sqrt{\frac{(J+m)!(J-m)!}{(J+k)!(J-k)!}} \sum_l \binom{J-k}{l} \binom{J+k}{J-m-l} s^{\frac{2l+k+m}{2}} (1-s)^{\frac{2J-m-k-2l}{2}} \quad (30)$$

$$= \sqrt{\frac{(J+m)!(J-m)! s^{J+k} (1-s)^{J-k}}{(J+k)!(J-k)!}} \sum_l \binom{J-k}{l} \binom{J+k}{J-m-l} \left(\frac{s}{1-s}\right)^{l-\frac{J-m}{2}} \quad (31)$$

$$\leq \sqrt{\binom{2J}{J+k} s^{J+k} (1-s)^{J-k}} \cdot \sqrt{\binom{2J}{J-m} \left(\frac{s}{1-s}\right)^{J-m}}, \quad (32)$$

and thus we have reached Eq. (26). Notice that the last inequality is for the case $s \geq 1/2$. For $s < 1/2$, the last term in the second square-root should be replaced by $[(1-s)/s]^{J-m}$. \square

Proof of Theorem 1. First observe that since $[U_\phi^{\otimes n}, P_{\text{proj}, J}] = 0$, the error is independent of ϕ . Then we can rewrite the error as

$$\begin{aligned} \epsilon_{\text{proj}, J} &\leq \frac{1}{2} \left\{ \|P_{\text{proj}, J} \rho_{p, J} P_{\text{proj}, J} - \rho_{p, J}\|_1 + (1 - \text{Tr}[P_{\text{proj}, J} \rho_{p, J}]) \right\} \\ &\leq \frac{1}{2} \left\{ 2\sqrt{(1 - \text{Tr}[P_{\text{proj}, J} \rho_{p, J}])} + (1 - \text{Tr}[P_{\text{proj}, J} \rho_{p, J}]) \right\} \\ &\leq \frac{3}{2} \sqrt{1 - \text{Tr}[P_{\text{proj}, J} \rho_{p, J}]}, \end{aligned}$$

having used the gentle measurement lemma [43, 44] to derive the second last inequality. We now simply have to estimate $1 - \text{Tr}[P_{\text{proj}, J} \rho_{p, J}]$. First, we expend the quantity as

$$\begin{aligned} 1 - \text{Tr}[P_{\text{proj}, J} \rho_{p, J}] &= \sum_{m=-J}^J \frac{p^{J+m} (1-p)^{J-m}}{N_J} \langle J, m|_s (I - P_{\text{proj}, J}) |J, m\rangle_s \\ &= \sum_{m=-J}^J \frac{p^{J+m} (1-p)^{J-m}}{N_J} \sum_{|k-(2s-1)J| > \frac{\sqrt{J \log J}}{2}} |\langle J, m|_s |J, k\rangle|^2. \end{aligned}$$

Applying Lemma 1 (for $s \geq 1/2$, and the case $s < 1/2$ can be treated in the same way), we have

$$\begin{aligned} 1 - \text{Tr}[P_{\text{proj}, J} \rho_{p, J}] &\leq \sum_{m=J-a}^J \frac{p^{J+m} (1-p)^{J-m}}{N_J} \left(\frac{s}{1-s}\right)^{J-m} \binom{2J}{J-m} \sum_{|k-(2s-1)J| > \frac{\sqrt{J \log J}}{2}} s^k (1-s)^{2J-k} \binom{2J}{k} \\ &\quad + \sum_{m=-J}^{J-a-1} \frac{p^{J+m} (1-p)^{J-m}}{N_J} \end{aligned}$$

where $a \geq 2$ is a parameter to be specified later. We continue bounding the term as

$$1 - \text{Tr} [P_{\text{proj},J} \rho_{p,J}] \leq \left(\frac{s}{1-s}\right)^a \binom{2J}{a} \sum_{|k-(2s-1)J| > \frac{\sqrt{J \log J}}{2}} s^k (1-s)^{2J-k} \binom{2J}{k} + \left(\frac{1-p}{p}\right)^{a+1} \quad (33)$$

$$\leq \frac{2(2J)^a}{a!} \exp \left[-\frac{\log^2 J}{4} + a \ln \left(\frac{s}{1-s} \right) \right] + \left(\frac{1-p}{p}\right)^{a+1} \quad (34)$$

$$\leq \exp \left[-\frac{\ln^2 J}{4 \ln^2 2} + a \ln(2J) + a \ln \left(\frac{s}{1-s} \right) \right] + \left(\frac{1-p}{p}\right)^{a+1}, \quad (35)$$

having used Hoeffding's bound and $a \geq 2$. Choosing, for instance, $a = \lfloor (\ln J)/4 \rfloor$ guarantees that

$$\begin{aligned} \epsilon_{\text{proj},J} &\leq \frac{3}{2} \sqrt{\exp \left[-\frac{\ln^2 J}{4 \ln^2 2} + \frac{\ln^2 J}{4} + \frac{\ln J}{4} \ln \left(\frac{s}{1-s} \right) \right] + \left(\frac{1-p}{p}\right)^{(\ln J)/4+1}} \\ &\leq \frac{3}{2} \left(\frac{1-p}{p}\right)^{(\ln J)/8} + O\left(J^{-\frac{1}{8} \ln J}\right) \\ &= (3/2) J^{-\frac{1}{8} \ln \left(\frac{p}{1-p}\right)} + O\left(J^{-\frac{1}{8} \ln J}\right). \end{aligned}$$

□

Appendix B: bound on the storage error.

Here we prove the compressor mentioned in the main text has a vanishing error. First, notice that the trace distance between the original state $\rho_{\phi,p}^{\otimes n}$ and the output of the compression protocol, denoted as $\rho'_{\phi,p,n}$, is

$$\begin{aligned} \epsilon_{\phi,p} &= \frac{1}{2} \left\| \rho'_{\phi,p,n} - \rho_{\phi,p}^{\otimes n} \right\|_1 \\ &= \frac{1}{2} \left\| \sum_J q_J |J\rangle\langle J| \otimes [\mathcal{P}_{\text{proj},J}(\rho_{\phi,p,J}) - \rho_{\phi,p,J}] \otimes \frac{I_{m_J}}{m_J} \right\|_1 \\ &= \sum_J q_J \cdot \epsilon_{\text{proj},J}, \quad \epsilon_{\text{proj},J} = \frac{1}{2} \left\| \mathcal{P}_{\text{proj},J}(\rho_{\phi,p,J}) - \rho_{\phi,p,J} \right\|_1. \end{aligned} \quad (36)$$

Since we already have a bound for $\epsilon_{\text{proj},J}$, the only ingredient needed for the error bound is the concentration property of q_J . Notice that the probability distribution q_J in Eq. (19) has the explicit form [45]

$$q_J = \frac{2J+1}{2J_0} \left[B\left(\frac{n}{2} + J + 1\right) - B\left(\frac{n}{2} - J\right) \right] \quad (37)$$

where $B(k) = p^k (1-p)^{n-k} \binom{n}{k}$ and $J_0 = (p-1/2)(n+1)$, which is a Gaussian distribution concentrated in an interval of width $O(\sqrt{n})$ around J_0 when n is large. Picking an interval much larger than \sqrt{n} , we get from Hoeffding's inequality that

$$\sum_{|J-J_0| \leq n^{2/3}} q_J \geq 1 - 2 \exp \left[-\frac{2n^{1/3}}{p^2} \right]. \quad (38)$$

Substituting the above inequality into Eq. (36), we have

$$\begin{aligned} \epsilon_{\phi,p} &\leq \max_{|J-J_0| \leq n^{2/3}} \epsilon_{\text{proj},J} + \sum_{|J-J_0| > n^{2/3}} q_J \\ &\leq \frac{3}{2} \left(\frac{2}{(2p-1)n}\right)^{\frac{1}{8} \ln \left(\frac{p}{1-p}\right)} + O\left(n^{-\frac{1}{8} \ln n}\right). \end{aligned}$$

Finally, substituting $p = (1 + e^{-\gamma t})/2$ into the above inequality, the error for the compressor in the depolarizing model is bounded by

$$\epsilon_{\gamma,t} \leq \frac{3}{2} \left(\frac{2e^{\gamma t}}{n} \right)^{\frac{1}{8} \ln \cosh \frac{\gamma t}{2}} + O\left(n^{-\frac{1}{8} \ln n}\right).$$

From the above bound, we can directly get the bound for the overall error of compression in a quantum stopwatch as

$$\epsilon_{T,\gamma}^{(k)} \leq \frac{3k}{2} \left(\frac{2e^{\gamma T}}{n} \right)^{\frac{1}{8} \ln \coth \frac{\gamma T}{2}} + O\left(kn^{-\frac{1}{8} \ln n}\right), \quad (39)$$

where k is the number of events and T is the total duration.

Appendix C: coherent versus incoherent protocols.

Here we compare the accuracy of the coherent protocols with the accuracy of incoherent protocols using repeated measurements.

Suppose that we want to measure the total duration of k intervals, each of which has length T/k . In the coherent protocol, each clock qubit starts with a pure state and ends up in a mixed state with maximum eigenvalue depending on the total duration T as $p(T, \gamma) = (1 + e^{-\gamma T})/2$. The inaccuracy for the quantum stopwatch thus has leading order $1/\sqrt{nF_{\text{loc}}}$, where

$$F_{\text{loc}} = 1 - \gamma^2 - \sqrt{1 - 4s(1-s)(2p-1)^2} + \frac{\gamma^2}{\sqrt{1 - 4s(1-s)e^{-2\gamma T}}}$$

is the classical Fisher information. On the other hand, an incoherent protocol involves k measurements of time and k initializations of the clock qubits, resulting in an of leading order $\sqrt{k/(nF'_{\text{loc}})}$, where F'_{loc} is the classical Fisher information of the individual step, given by

$$F'_{\text{loc}} = 1 - \gamma^2 - \sqrt{1 - 4s(1-s)e^{-2\gamma T/k}} + \frac{\gamma^2}{\sqrt{1 - 4s(1-s)e^{-2\gamma T/k}}}.$$

Comparing the two error terms, we conclude that the coherent protocol outperforms the incoherent one when $F_{\text{loc}} \geq (F'_{\text{loc}})/k$. Since $F_{\text{loc}} \geq 1 - \sqrt{1 - 4s(1-s)e^{-2\gamma T}}$ and $F'_{\text{loc}} \leq 1 + \gamma^2/\sqrt{1 - 4s(1-s)}$. A sufficient condition for this condition is

$$k \left[1 - \sqrt{1 - 4s(1-s)e^{-2\gamma T}} \right] \geq 1 + \frac{\gamma^2}{\sqrt{1 - 4s(1-s)}}$$

The last inequality implies the condition $k \geq \left(1 + \gamma^2/\sqrt{1 - 4s(1-s)}\right) / \left(1 - \sqrt{1 - 4s(1-s)e^{-2\gamma T}}\right)$, indicating that the coherent protocol has an advantage whenever the number of events is sufficiently large.

Appendix D: Quantum Fisher Information of the clock states.

We derive the Quantum Fisher Information (QFI) for the estimation of T from the state $\rho_{T,\gamma}$. To this purpose, we first calculate the symmetric logarithmic derivative (SLD) operator $L_{T,\gamma}$, defined by the equation

$$\frac{d\rho_{T,\gamma}}{dT} = \frac{1}{2}(L_{T,\gamma} \rho_{T,\gamma} + \rho_{T,\gamma} L_{T,\gamma}). \quad (40)$$

In the time-varying frame $\{|\varphi_T\rangle, |\varphi_T^\perp\rangle\}$, the SLD takes the form

$$L_{T,\gamma} = -\frac{\gamma}{1 + e^{\gamma T}} |\varphi_T\rangle\langle\varphi_T| - 2\sqrt{s(1-s)}e^{-\gamma T} \left(i|\varphi_T\rangle\langle\varphi_T^\perp| - i|\varphi_T^\perp\rangle\langle\varphi_T| \right) + \frac{\gamma}{e^{\gamma T} - 1} |\varphi_T^\perp\rangle\langle\varphi_T^\perp|. \quad (41)$$

Then, the quantum Fisher information for $\rho_{T,p}$ can be evaluated as

$$\begin{aligned} F_Q &= \text{Tr} [(L_{T,p})^2 \rho_{T,p}] \\ &= 4s(1-s)e^{-2\gamma T} + \frac{\gamma^2}{e^{2\gamma T} - 1}. \end{aligned} \quad (42)$$

Appendix E: comparison between the local strategy and the optimal strategy.

The ratio between the inaccuracies of the local strategy and the optimal strategy is given by the inverse ratio between the square roots of the Fisher informations, up to an $O(n^{-1})$ term. For the ratio between the Fisher informations, we have

$$\frac{F_Q}{F_{\text{loc}}} = \frac{4s(1-s)e^{-2\gamma T} + \frac{\gamma^2}{e^{2\gamma T} - 1}}{\left[1 - \sqrt{1 - 4s(1-s)e^{-2\gamma T}}\right] \left[1 + \frac{\gamma^2}{\sqrt{1 - 4s(1-s)e^{-2\gamma T}}}\right]}. \quad (43)$$

By elementary algebra, we obtain the following lower bound

$$\begin{aligned} \frac{F_Q}{F_{\text{loc}}} &= \frac{4s(1-s)e^{-2\gamma T}}{1 - \sqrt{1 - 4s(1-s)e^{-2\gamma T}}} \cdot \frac{1 + \gamma^2/[4s(1-s)(1 - e^{-2\gamma T})]}{1 + \gamma^2/\sqrt{1 - 4s(1-s)e^{-2\gamma T}}} \\ &\geq 2 \cdot \frac{1 + \gamma^2/[4s(1-s)(1 - e^{-2\gamma T})]}{1 + \gamma^2/\sqrt{1 - 4s(1-s)e^{-2\gamma T}}} \end{aligned} \quad (44)$$

Assuming that the time $T \geq T_{\min} > 0$, we obtain the lower bound

$$\frac{F_Q}{F_{\text{loc}}} \geq 2 \cdot \frac{1 + \gamma^2/[4s(1-s)(1 - e^{-\gamma T_{\min}})]}{1 + \gamma^2}. \quad (45)$$

Note that the r.h.s. is equal to $1/2$ in the noiseless case $\gamma = 0$.

Appendix F: accuracy of the local strategy for unknown γ .

Here we analyze the precision of local time measurement strategy when γ is unknown and is treated as a nuisance parameter, which is not directly of interest but affects the analysis of our estimation. For this analysis, we parameterize the distribution of our interest as $P_{T,\gamma}(\tau)$ because the dependence on γ is crucial in the following discussion. Then, we introduce Fisher information matrix F_{loc} defined by

$$(F_{\text{loc}})_{x,y} := \int_0^{2\pi} d\tau \frac{\partial \log P_{T,\gamma}(\tau)}{\partial x} \cdot \frac{\partial \log P_{T,\gamma}(\tau)}{\partial y} P_{T,\gamma}(\tau),$$

where $x, y \in \{T, \gamma\}$. And we need to evaluate $(F_{\text{loc}}^{-1})_{TT}$, namely the (T, T) -entry of the inverse Fisher information matrix F_{loc}^{-1} .

To simplify the calculation, we first adapt a re-parameterization of the nuisance parameter from γ to $p = (e^{-\gamma T} + 1)/2$. The T component $(F_{\text{loc}}^{-1})_{TT}$ of the inverse Fisher information is invariant under such a re-parameterization of the nuisance parameter, which can be proved as follows.

The inverse Fisher information F_{loc}^{-1} with respect to the parametrization (T, γ) is given by

$$F_{\text{loc}}^{-1} = \begin{bmatrix} (F_{\text{loc}})_{TT} & (F_{\text{loc}})_{T,\gamma} \\ (F_{\text{loc}})_{\gamma,T} & (F_{\text{loc}})_{\gamma\gamma} \end{bmatrix}^{-1}.$$

Now, consider a re-parameterization of the nuisance parameter $\gamma \rightarrow p$, and the new Fisher information matrix is

$$F_{\text{loc},p}^{-1} = A^T F_{\text{loc}}^{-1} A$$

where

$$A = \begin{pmatrix} 1 & 0 \\ \frac{\partial \gamma}{\partial T} & \frac{\partial \gamma}{\partial p} \end{pmatrix}$$

is the Jacobi matrix. Therefore, we have

$$F_{\text{loc}}^{-1} = A \left(F_{\text{loc},p}^{-1} \right) A^T$$

and it can be checked by straightforward calculation that

$$(F_{\text{loc}}^{-1})_{TT} = (F_{\text{loc},p}^{-1})_{TT}.$$

It is therefore enough to calculate the Fisher information matrix for the parameterization (T, p) , when the input state is $\rho_{T,p} = p|\varphi_T\rangle\langle\varphi_T| + (1-p)|\varphi_T^\perp\rangle\langle\varphi_T^\perp|$ with $|\varphi_T\rangle = \sqrt{s}|0\rangle + \sqrt{1-s}e^{-iT}|1\rangle$ and $|\varphi_T^\perp\rangle = \sqrt{1-s}|0\rangle - \sqrt{s}e^{-iT}|1\rangle$. That is, in the following, we employ the parametrization $P_{T,p}(\tau)$ by the pair (T, p) for the probability of the measurement to yield outcome τ . When the input state is $\rho_{T,p}$, it can be expressed as

$$\begin{aligned} P_{T,p}(\tau) &:= \text{Tr}[\rho_{T,p}M_\tau] \\ &= \frac{1}{2\pi}(1 + 2(2p-1)\sqrt{s(1-s)}\cos(\tau-T)). \end{aligned} \quad (46)$$

The Fisher information of $P_{T,p}(\tau)$ can be derived from a lengthy but straightforward calculation, and we have

$$\begin{aligned} (F_{\text{loc},p})_{TT} &= \int_0^{2\pi} \left(\frac{\partial \log P_{T,p}(\tau)}{\partial T} \right)^2 P_{T,p}(\tau) d\tau \\ &= 1 - \sqrt{1 - 4s(1-s)(2p-1)^2} \\ &= 1 - \sqrt{1 - 4s(1-s)e^{-2\gamma T}}. \end{aligned} \quad (47)$$

To evaluate the inverse of the Fisher information matrix, we also need to calculate the off-diagonal elements. We define the logarithmic likelihood derivative $l_p(\tau)$ with respect to p as

$$\begin{aligned} l_p(\tau) &:= \frac{\partial \log P_{T,p}(\tau)}{\partial p} \\ &= \frac{4\sqrt{s(1-s)}\cos(\tau-T)}{1 + 2(2p-1)\sqrt{s(1-s)}\cos(\tau-T)}. \end{aligned}$$

Then the off-diagonal components $F_{T,p}$ and $F_{p,T}$ are given as

$$(F_{\text{loc},p})_{T,p} = (F_{\text{loc},p})_{p,T} := \int_0^{2\pi} l_p(\tau) \frac{\partial \log P_{T,p}(\tau)}{\partial T} P_{T,p}(\tau) d\tau = 0. \quad (48)$$

Since the off-diagonal components are zero, we have

$$(F_{\text{loc}}^{-1})_{TT} = (F_{\text{loc},p}^{-1})_{TT} = 1 / (F_{\text{loc},p})_{TT}.$$

The value of $(F_{\text{loc}}^{-1})_{TT}$ is thus given by the reciprocal of the r.h.s. of Eq. (47).

Appendix G: evaluation of the inverse quantum Fisher information for unknown γ .

Here we evaluate the inverse quantum Fisher information for unknown γ . By the same argument as in the previous section, we can re-parameterize the nuisance parameter as $p = (e^{-\gamma T} + 1)/2$ without affecting $(F_{\text{Q}}^{-1})_{TT}$. We denote by $F_{Q,p}$ the quantum Fisher information matrix under the parameterization (T, p) , which is defined as

$$(F_{Q,p})_{x,y} := \text{Tr} \left[\left(\frac{L_x L_y + L_y L_x}{2} \right) \rho_{T,p} \right],$$

where $x, y \in \{T, p\}$ and L_x, L_y are the SLD operators.

We first calculate $(F_{Q,p})_{TT}$ for the quantum information matrix under the parameterization (T, p) . The symmetry of the problem implies that value $F_{Q,p}$ does not depend on T . Solving the equation $\frac{\partial \rho_{T,p}}{\partial T} = \frac{1}{2}(\rho_{T,p}L_T + L_T\rho_{T,p})$ for $T = 0$, we get the symmetric logarithmic derivative for T at $T = 0$ as

$$(L_T)_{T=0} = 2(2p-1)\sqrt{s(1-s)} \begin{pmatrix} 0 & -i \\ i & 0 \end{pmatrix}.$$

Then we have

$$\begin{aligned} (F_{Q,p})_{TT} &:= \text{Tr} [L_T^2 \rho_{T,p}] = 4s(1-s)(2p-1)^2 \\ &= 4s(1-s)e^{-2\gamma T}. \end{aligned} \tag{49}$$

In a similar way, we get the symmetric logarithmic derivative for p at $T=0$ as

$$(L_p)_{T=0} = \frac{1}{p(1-p)} \begin{pmatrix} s-p & \sqrt{s(1-s)} \\ \sqrt{s(1-s)} & 1-s-p \end{pmatrix}.$$

The off-diagonal elements of the quantum Fisher information matrix can be evaluated as

$$(F_{Q,p})_{T,p} = (F_{Q,p})_{p,T} := (1/2) \text{Tr} [(L_T L_p + L_p L_T) \rho_{T,p}] = 0. \tag{50}$$

Since the off-diagonal components are zero, we have

$$\left(F_Q^{-1}\right)_{TT} = \left(F_{Q,p}^{-1}\right)_{TT} = 1/(F_{Q,p})_{TT},$$

which is given by the reciprocal of the r.h.s. of Eq. (49).
